

Quasibound states and heteroclinic structures in the driven Morse potential

Daungruthai Jarukanont, Kyungsun Na, and L. E. Reichl

Center for Complex Quantum Systems and Department of Physics, The University of Texas at Austin, Austin, Texas 78712, USA

(Received 14 November 2006; published 2 February 2007)

We have studied the classical and quantum dynamics of the Morse system driven by time-periodic external field. Floquet energies and Husimi probability distributions of quasibound states of the driven system are obtained using exterior complex scaling method and Floquet theory. As we increase the external field strength, the number of quasibound states is decreased and the Husimi distribution of the quasibound state shows the enhanced positive momentum distribution that appears to be supported by the classical homoclinic tangles that develop on the positive momentum side of the phase space.

DOI: [10.1103/PhysRevA.75.023403](https://doi.org/10.1103/PhysRevA.75.023403)

PACS number(s): 32.80.Rm, 05.45.Mt

I. INTRODUCTION

The interaction between electrons confined to atomic or molecular potentials and laser radiation can give rise to unexpected behavior such as stabilization of electron states [1–3]. Stabilization involves decreasing probability of ionization of an electron with increasing laser intensity. For linearly polarized incident radiation, simple one-dimensional (1D) models of the atomic or molecular potential are often sufficient to describe the dominant behavior of the irradiated system [4–7].

Two 1D potentials that have been used extensively to study the dynamics of the laser-matter interaction are the inverted Gaussian potential [8–14] and the Morse potential [15–20,11]. Although the spatial variation of the potential energy is very different for these two potentials, they have the same energy spectrum. The inverted Gaussian potential has symmetry under $x \rightarrow -x$. The Morse potential has an infinitely high barrier as $x \rightarrow -\infty$.

In the presence of laser radiation, bound states become quasibound states, although the tightly bound states may have such a long lifetime that they effectively remain bound states. In addition, for the inverted Gaussian potential, the laser radiation can create new quasibound states, some of which have very long lifetimes [13]. Electron stabilization in the presence of radiation means that the lifetimes of some key field-induced quasibound states become longer with increasing field intensity. Therefore the behavior of quasibound states becomes the key to understanding electron stabilization.

In both the inverted Gaussian potential and the Morse potential, radiation induces chaos in the underlying classical phase space. As the strength of the radiation field increases the phase space becomes more and more dominated by chaotic orbits and heteroclinic tangles that can extend far out into asymptotic regions of the classical phase space [20,13,14]. There are several ways to obtain information about quasi-bound states in the presence of monochromatic radiation. All are based on the use of Floquet theory since the Hamiltonian of such systems is time-periodic. One of the most common methods is to use complex coordinate rotation [21,22] which has the effect of rotating the continuum Floquet eigenvalues in the complex plane but leaves the positions of the complex poles associated with quasibound states

unchanged. Timberlake and Reichl [12] used this method to obtain Husimi plots of residues of quasibound states in the inverted Gaussian potential and found that they appeared to form “scars” on unstable periodic orbits in the classical phase space. In Refs. [11,12] it is shown that complex Floquet energies can undergo avoided crossings in the complex energy plane. A second method for locating quasi-bound states uses the more recently developed Floquet scattering theory. Emmanouilidou and Reichl [13] used this method to show the creation of a radiation induced quasibound state with increasing field intensity for the driven inverted Gaussian system. They also found that the external field created a significant chaotic structure in the classical phase space of the inverted Gaussian potential.

The driven Morse system has also been studied extensively but the effect of chaos on quasibound states has not been addressed. Ben-Tal *et al.* [11] studied the formation of quasibound states in the driven Morse potential and unlike the inverted Gaussian they show that creation of new quasibound states with increasing driving field intensity does not appear to occur in the driven Morse potential. However, they do not study the influence of underlying classical dynamics on the quasibound states of this system. Jung [20] has found scattering chaos in the driven Morse system. He explained this in terms of the heteroclinic structure of unstable periodic orbits.

In this paper we use the complex coordinate rotation method to show that heteroclinic tangles in the driven Morse potential do appear to influence the spatial structure of quasibound states. This is similar to work of Lee *et al.* [23] showing that quasibound states can be stabilized by chaotic tangles in electron waveguide structures. In Sec. II, we write the Hamiltonian for the driven Morse system. The energy eigenstates for the nondriven Morse system will form the basis states for studying the driven case. Therefore, in Sec. II, we also list the field-free Morse eigenstates for the bound states and the continuum states. We will use Floquet theory and complex scaling to obtain the energies and probability distributions of quasibound states. In Sec. III, we explore the classical dynamics of the driven Morse system in both the low frequency and high frequency regimes. We find large regions of the classical phase space; in the region of influence of the Morse potential, to be dominated by homoclinic tangles and chaos. In Sec. IV, we use the Floquet theory and the exterior complex scaling method to find quasibound

states. The complex Floquet eigenvalues, Floquet eigenstates, and the lifetime of the quasibound states are obtained. We study the phase space distributions of the quasibound states represented by Husimi distribution. Finally, in Sec. V we make some concluding remarks.

II. THE DRIVEN MORSE SYSTEM

We consider an electron in a potential well, which we model in terms of the Morse potential, driven by a time periodic radiation field. We use the same parameters as in Refs. [11,26] which model the dynamics of the valence electron in xenon. The Hamiltonian for the driven system, in atomic units, is given by

$$\hat{H}(t) = \frac{1}{2} \left[\hat{p} - \frac{\varepsilon_0}{\omega} \sin(\omega t) \right]^2 + D(e^{-2\alpha\hat{x}} - 2e^{-\alpha\hat{x}}), \quad (1)$$

where \hat{p} and \hat{x} are momentum and position operators, respectively. We use atomic units throughout this paper (the reduced mass of the electron, $\mu=1$ a.u. and Planck constant $\hbar=1$ a.u.). $D=0.6643$ a.u. is the ‘‘depth’’ of the Morse potential and the parameter $\alpha=0.417$ a.u. controls the ‘‘width’’ of the potential. The radiation field has strength ε_0 and frequency ω . These parameters allow us to reproduce the lowest two energy states of the valence electron in xenon at $E_1=-0.4457$ a.u., $E_2=-0.1389$ a.u. and a third weakly bound state at $E_3=-0.0061$ a.u.

A. Floquet theory [24]

The solutions, $|\psi(t)\rangle$, to the Schrödinger equation

$$i \frac{\partial}{\partial t} |\psi(t)\rangle = \hat{H}(t) |\psi(t)\rangle \quad (2)$$

can be expanded in Floquet eigenstates $|\phi_\alpha(t)\rangle$ so that

$$|\psi(t)\rangle = \sum_\alpha A_\alpha e^{-i\Omega_\alpha t} |\phi_\alpha(t)\rangle. \quad (3)$$

The Floquet eigenstates are time-periodic $|\phi_\alpha(t)\rangle = |\phi_\alpha(t+T)\rangle$, where T is the period of the Hamiltonian Eq. (1). They satisfy the eigenvalue equation

$$\left[H(t) - i \frac{\partial}{\partial t} \right] |\phi_\alpha(t)\rangle = \Omega_\alpha |\phi_\alpha(t)\rangle \quad (4)$$

where Ω_α is the α th Floquet eigenphase. The Floquet eigenstates $|\phi_\alpha(t)\rangle$ form a complete orthogonal-normal set.

At the time $t=T$, the solution to the Schrödinger equation can be written

$$|\psi(T)\rangle = \sum_\alpha e^{-i\Omega_\alpha T} |\phi_\alpha(0)\rangle \langle \phi_\alpha(0) | \psi(0)\rangle. \quad (5)$$

From Eq. (5), the Floquet evolution operator at time $t=T$ is defined as

$$\hat{U}(T) = \sum_\alpha e^{-i\Omega_\alpha T} |\phi_\alpha(0)\rangle \langle \phi_\alpha(0) |. \quad (6)$$

The eigenvalues and eigenstates of the Floquet evolution operator $\hat{U}(T)$ can be computed numerically by evaluating $\hat{U}(T)$

using as a basis the energy eigenstates, $|\chi_m\rangle$, of the unperturbed Morse system

$$U_{n,m}(T) = \sum_\alpha e^{-i\Omega_\alpha T} \langle \chi_n | \phi_\alpha(0)\rangle \langle \phi_\alpha(0) | \chi_m\rangle. \quad (7)$$

If we diagonalize the Floquet matrix in Eq. (7), we obtain the eigenvalues $e^{-i\Omega_\alpha T}$ and eigenstates of $\hat{U}(T)$ in terms of the Morse energy eigenstates such that

$$|\phi_\alpha(T)\rangle = |\phi_\alpha(0)\rangle = \sum_n c_n |\chi_n\rangle. \quad (8)$$

The Floquet matrix in Eq. (7) is computed by writing the Schrödinger equation in terms of a basis set composed of the Morse energy eigenstates. We then integrate the Schrödinger equation for one period of time using one of the Morse energy eigenstates as an initial condition. This gives one column of the Floquet time evolution matrix. This process is repeated for each energy eigenstate until the full Floquet matrix is constructed.

B. Energy eigenstates for the unperturbed morse system

The eigenvalue equation for energy eigenstates of the unperturbed Morse system can be written

$$E_n \chi_n(x) = -\frac{1}{2} \frac{\partial^2 \chi_n(x)}{\partial x^2} + D(e^{-2\alpha x} - 2e^{-\alpha x}) \chi_n(x), \quad (9)$$

where E_n is the n th energy eigenvalue and $\chi_n(x)$ is the n th energy eigenfunction. This system contains both bound states and continuum states and below we discuss them separately.

Bound state solutions. The bound state eigenfunctions can be written [27]

$$\chi_n(x) = N_n e^{-z/2} z^{b_n} L_n^{b_n}(z), \quad (10)$$

where $L_n^{b_n}(z)$ is the Laguerre polynomial, $z=2ae^{-\alpha x}$, $a = \sqrt{2D/\alpha}$, $b_n = \sqrt{-2E_n}/\alpha$, and the normalization constant is $N_n = \sqrt{\frac{\alpha(2a-1-2n)!}{\Gamma(2a-n)}}$, where $\Gamma(x)$ is the Γ function. The energy eigenvalues are given by

$$E_n = -D - 2\alpha\sqrt{D/2} \left(n + \frac{1}{2} \right) - (\alpha^2/2) \left(n + \frac{1}{2} \right)^2. \quad (11)$$

The Morse potential for $D=0.6643$ a.u. and $\alpha=0.417$ a.u. is shown in Fig. 1. For these parameters, the Morse potential has three bound states. The probability distributions of these three bound states are also shown in Fig. 1.

It is useful also to look at Husimi plots of these energy eigenstates. The Husimi function for the energy eigenstate $\chi_n(x)$ can be written [25]

$$G(q,p) = \frac{1}{2\pi} \left| \left(\frac{1}{2\pi\sigma^2} \right)^{1/4} \int_{-\infty}^{\infty} e^{(x'-x)^2/2\sigma^2 - ipx'} \chi_n(x') dx' \right|^2, \quad (12)$$

where σ is a coarse-graining parameter that determines the width of the Gaussian in the x and p directions. By calculating these Husimi distributions we can visualize how the probability distribution associated with a given quantum

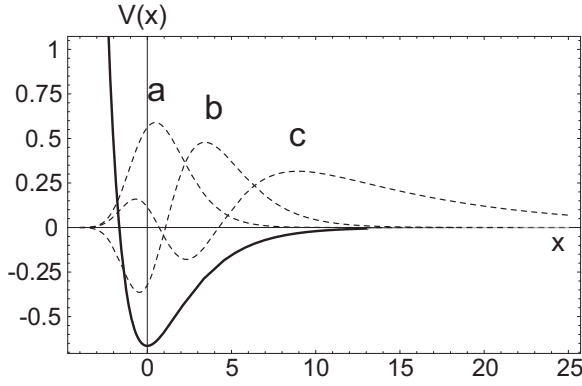


FIG. 1. The Morse potential for parameters $D=0.6643$ a.u. and $\alpha=0.417$ a.u. (the solid line). The probability distribution of the three bound states corresponding to the energies (a) $E_1=-0.4457$ a.u., (b) $E_2=-0.1389$ a.u. and the third weakly bound state energy (c) $E_3=-0.0061$ a.u.

state is distributed in phase space. These phase space structures can then be compared with structures in a strobe plot of the classical phase space. Husimi plots of the three bound states of the Morse system we are considering are shown in Fig. 2 for $\sigma=0.9$.

Continuum eigenstates. The continuum energy eigenstates for the Morse system in Eq. (9) are [27]

$$\chi_\varepsilon(x) = C_\varepsilon e^{-z/2} [A(\varepsilon) z^{i\varepsilon} F(-s+i\varepsilon, 2i\varepsilon+1; z) + A^*(\varepsilon) z^{-i\varepsilon} F(-s-i\varepsilon, -2i\varepsilon+1; z)], \quad (13)$$

where $F(-s+i\varepsilon, 2i\varepsilon+1; z)$ is the confluent hypergeometric function of the first kind, $2s=2a-1$, and $A(\varepsilon)=\Gamma(-2i\varepsilon)/\Gamma(-s-i\varepsilon)$. The normalization constant is $C_\varepsilon = \frac{\sqrt{\alpha}}{\sqrt{2\pi|A(\varepsilon)|}}$, where

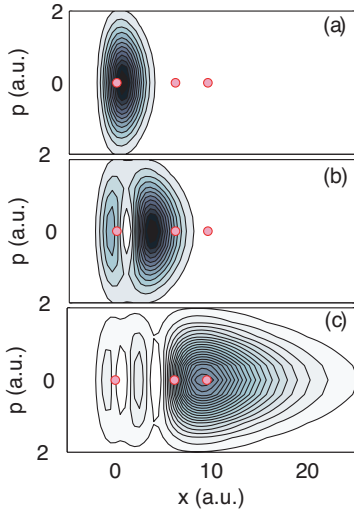


FIG. 2. (Color online) Husimi distributions of the three bound states of the unperturbed Morse system at energies (a) $E_1=-0.4457$ a.u., (b) $E_2=-0.1389$ a.u. and (c) $E_3=-0.0061$ a.u. These states were calculated using $\alpha=0.417$ a.u., $D=0.6643$ a.u., and $\sigma=0.9$. The small filled circles along the $p=0$ axis are period-1 periodic orbits in the classical phase space.

the energy E of the continuum states is related to ε as $\varepsilon = \sqrt{2E/\alpha} = k/\alpha$. $A^*(\varepsilon)$ is a complex conjugate of $A(\varepsilon)$ and k is the wave number. The orthonormality of the eigenfunctions $\chi_n(x)$ in Eq. (10) and $\chi_\varepsilon(x)$ in Eq. (13) is established in Ref. [27].

C. Complex coordinate scaling

For the Morse system, which allows ionization, the external field will turn the bound states into quasi-bound states with finite life time and complex energy

$$E_{\text{res}} = E_R - i\Gamma/2, \quad (14)$$

where E_R and Γ are real, $\Gamma \geq 0$ and $\tau=1/\Gamma$ is the lifetime of the state. Complex quasibound state energies occur as poles in the complex energy plane of the Green's function of the system. True bound states occur as poles on the real energy axis. Continuum states form a cut along the real energy axis. The bound state poles have residues which are composed of the energy eigenstates associated with the bound states. These functions are bounded in space. The quasibound states have residues which are unbounded in space. The complex scaling technique rotates the cut associated with the continuum states into the complex energy plane in the lower half complex plane by the factor $e^{-2i\theta}$ but does not change the position of the quasibound state poles.

The complex coordinate scaling technique has been widely used in open quantum systems to determine the lifetime of quasibound states [21,22]. There are two approaches to complex scaling. One approach, the standard complex coordinate scaling (CCS) method involves rotation of the coordinate along the entire x axis so that $x \rightarrow xe^{i\theta}$. The other approach, the exterior complex coordinate scaling (ECCS) method rotates the coordinate x , but only in the region outside the influence of the potential. We shall use ECCS in our analysis of the driven Morse system.

The basic idea of ECCS is to scale the x coordinate by the factor $e^{i\theta}$, but only in the region $|x| \geq x_s$ where the potential is zero. The discontinuity at $x = \pm x_s$ is avoided by using a smooth scaling relation $x \rightarrow \tilde{x}$, where

$$x \rightarrow \tilde{x} = x + (e^{i\theta} - 1) \left[x + \frac{1}{2\lambda} \ln \left(\frac{\cosh[\lambda(x-x_s)]}{\cosh[\lambda(x+x_s)]} \right) \right]. \quad (15)$$

In this paper, we use $\lambda=5$ and $x_s=35$ a.u. The scaled coordinate $\tilde{x} \rightarrow x$ for $|x| \leq x_s$, and $\tilde{x} \rightarrow xe^{i\theta}$ for $x \rightarrow \infty$.

Under this transformation the Hamiltonian for the exterior complex scaled undriven Morse system is given by

$$\tilde{H}_0(x) = H_0(x) + V_{CAP}(x), \quad (16)$$

where $H_0(x)$ is the time-independent unscaled Hamiltonian of the Morse system for which we already have the analytic expressions for the bound and continuum eigenvalues:

$$V_{CAP}(x) = V_0(x) + V_1(x) \frac{\partial}{\partial x} + V_2(x) \frac{\partial^2}{\partial x^2}, \quad (17)$$

$$V_0(x) = \frac{f^{-3}}{4} \frac{\partial^2 f}{\partial x^2} - \frac{5}{8} f^{-4} \left(\frac{\partial f}{\partial x} \right)^2, \quad (18)$$

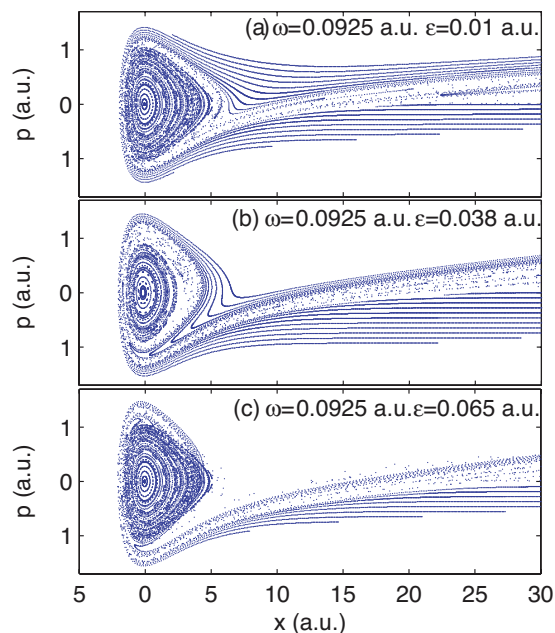


FIG. 3. (Color online) Strobe plots of the driven Morse system for $\omega=0.0925$ a.u. with (a) $\epsilon=0.01$ a.u., (b) $\epsilon=0.038$ a.u., and (c) $\epsilon=0.065$ a.u. Lines of initial conditions with $p \leq 0$ constant (and differing in energy by integer units of $\hbar\omega$) and x in the asymptotic region and in the neighborhood of $x=0$ are used to generate this plot.

$$V_1(x) = f^{-3}(x) \frac{\partial f(x)}{\partial x}, \quad (19)$$

and

$$V_2(x) = \frac{1}{2}[1 - f^{-2}(x)]. \quad (20)$$

In all these expressions $f(x) = \partial \tilde{x} / \partial x$.

III. CLASSICAL DYNAMICS OF THE DRIVEN MORSE SYSTEM

The unperturbed Morse system is integrable. However, when the external field was turned on, the system can undergo a transition to chaos in some regions of the phase space. We can represent the dynamics of the driven system by strobe plots (Poincaré surface of section plots) [24]. Since our time-dependent Hamiltonian $H(x, p, t)$ is periodic in time, $H(x, p, t) = H(x, p, t+T)$, where T is the period of the driving field, the strobe plot can be obtained by plotting p and x at each period T of the external field [24]. We solve Hamilton's equations of motion to get $p(nT)$ and $x(nT)$, where $n = 1, 2, 3, \dots$

In our study of the driven system, we will use the Hamiltonian in Eq. (1) with the field strengths $\epsilon=0.01, 0.038$, and 0.065 a.u. Figure 3 shows strobe plots of the classical dynamics for these three field strengths and frequency $\omega = 0.0925$ a.u. In each plot, several lines of initial conditions with constant momentum and a range of values of x in the asymptotic region are used such that the energies of these

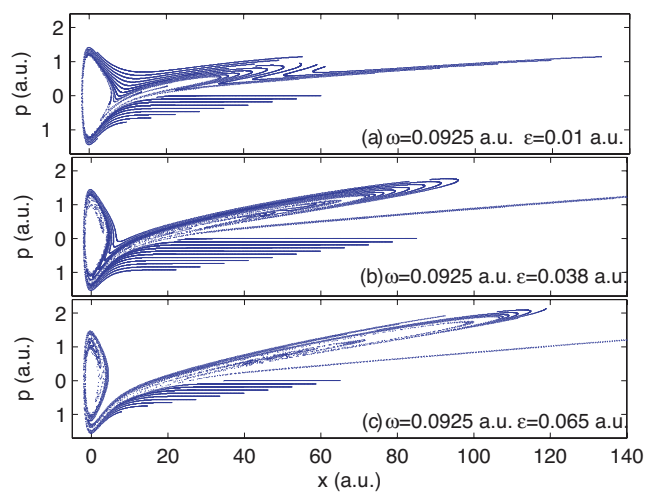


FIG. 4. (Color online) Strobe plots of the driven Morse system for $\omega=0.0925$ a.u. with (a) $\epsilon=0.01$ a.u., (b) $\epsilon=0.038$ a.u., and (c) $\epsilon=0.065$ a.u. Only lines of initial conditions with $p \leq 0$ constant and x in the asymptotic region are used. These lines of initial conditions differ in energy by integer units of $\hbar\omega$.

lines of initial conditions differ by photon energy $\hbar\omega$ (in atomic units). Since the Morse potential has a high potential wall for $x < 0$ all initial conditions have negative momentum and the trajectories emerge with positive momentum. In addition to the initial conditions in the asymptotic region, some initial conditions are taken for $p=0$ in the neighborhood of $x=0$ and show remaining Kolmogorov-Arnold-Moser (KAM) orbits from the interior of the Morse potential. In Fig. 4, we show the same plots but only using the lines of initial conditions in the asymptotic region and we show the orbits for a greater range of values of p and x . What is interesting about these plots is that there is a very large heteroclinic tangle that extends far into the asymptotic regions and only for positive momentum.

It is interesting to look at larger values of frequency and field intensity. In Fig. 5 we show strobe plots for $\omega = 2.0$ a.u. and field strengths $\epsilon=20$ a.u. and $\epsilon=30$ a.u. The central trapping region of the Morse potential still shows a stable periodic orbit surrounded by an island of stable KAM tori, but this stable trapping region has moved far out along the x axis. Also the structure of the heteroclinic tangles is more complex. These figures show fans of tangles coming off the central trapping region. In Fig. 5(a) the left-most tangle ends at about $(p=10, x=23)$. In Fig. 5(b) the left-most tangle ends at about $(p=12, x=30)$.

IV. QUANTUM DYNAMICS OF THE DRIVEN MORSE SYSTEM

Let us now use Floquet theory and the exterior complex coordinate scaling method (ECCS) to find the quasibound states in the driven Morse system. To observe the phase space structure of those quasibound states, we will examine their Husimi distributions. The ECCS method rotates the coordinate only when $x > x_s$, where $x_s = 35$ a.u. in all our calculations. There will be no complex coordinate scaling in the

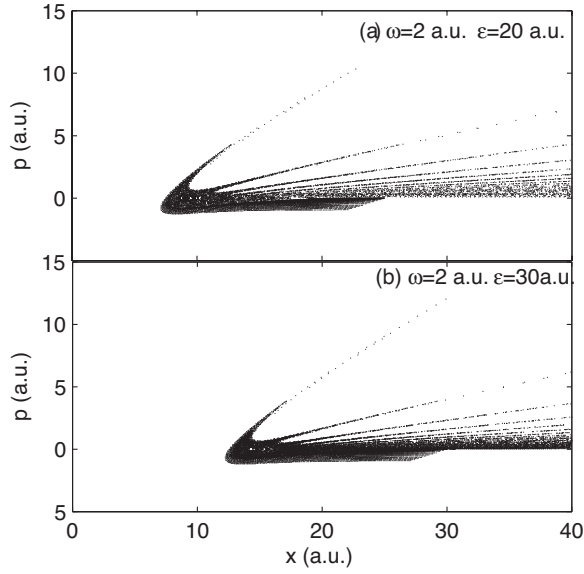


FIG. 5. Strobe plots of the driven Morse system for $\omega = 2.0$ a.u. with (a) $\varepsilon = 20.0$ a.u. and (b) $\varepsilon = 30.0$ a.u. Lines of initial conditions with $p \leq 0$ constant (and differing in energy by integer units of $\hbar\omega$) and x in the asymptotic region are used to generate this plot.

region around the potential. This allows us to see the Husimi distribution of the quasibound states without distortion resulting from scaling for $x < x_s$.

Following the ECCS method we introduced in Sec. II, the scaled Hamiltonian of the Morse system interacting with an external monochromatic field becomes

$$\tilde{H}(x, t) = \tilde{H}_0(x) - \frac{\varepsilon_0}{\omega} \tilde{p} \sin(\omega t) + \frac{\varepsilon_0^2}{2\omega^2} \sin^2(\omega t), \quad (21)$$

where

$$\tilde{H}_0(x) = H_0(x) + V_{CAP}(x) \quad (22)$$

with $V_{CAP}(x)$ given in Eq. (17).

The scaled time-independent eigenstates $|\xi_n\rangle$ of the unperturbed scaled Morse system $\tilde{H}_0(x)$ can be used as a basis to compute the Floquet evolution matrix $U(T)$ for the driven system. The time-dependent scaled Schrödinger equation for the driven Morse system is

$$i \frac{\partial}{\partial t} |\Psi(t)\rangle = \tilde{H}_0 |\Psi(t)\rangle - \frac{\varepsilon_0}{\omega} \tilde{p} \sin(\omega t) |\Psi(t)\rangle + \frac{\varepsilon_0^2}{2\omega^2} \sin^2(\omega t) \times |\Psi(t)\rangle. \quad (23)$$

We can expand the state $|\Psi(t)\rangle$ in terms of the unperturbed basis

$$|\Psi(t)\rangle = \sum_{j=1}^N a_j(t) |\xi_j\rangle, \quad (24)$$

where $a_j(t) = \langle \xi_j | \Psi(t) \rangle$ is the probability amplitude to find the system in the j th energy level of the scaled system at time t .

From Eq. (24), we can rewrite the time-dependent Schrödinger equation in the form

$$i \frac{\partial}{\partial t} a_j(t) = \tilde{E}_j a_j(t) - \frac{\varepsilon_0}{\omega} \sin(\omega t) \sum_{i=1}^N \tilde{p}_{j,i} a_i(t) + \frac{\varepsilon_0^2}{2\omega^2} \sin^2(\omega t) a_j(t), \quad (25)$$

where \tilde{E}_j is the j th eigenvalue of \tilde{H}_0 and $\tilde{p}_{j,i}$ is the dipole matrix element in the scaled energy basis defined by

$$\tilde{p}_{j,i} = \langle \xi_j | \tilde{p} | \xi_i \rangle = \sum_{m=1}^N \sum_{n=1}^N c_{m,i} c_{n,j} \langle \chi_m | \tilde{p} | \chi_n \rangle, \quad (26)$$

where we use the fact that $|\xi_j\rangle$ is expanded in terms of the unscaled time-independent Morse eigenstates $|\chi_n\rangle$, as $|\xi_j\rangle = \sum_{n=1}^N c_n |\chi_n\rangle$ and $\langle \xi_i | = \sum_{n=1}^N c_n \langle \chi_n |$ with the bilinear normalization condition $\sum_{n=1}^N c_n^2 = 1$. This normalization results from the fact that the scaled unperturbed Morse Hamiltonian is not Hermitian. Using the expression for the scaled momentum operator \tilde{p} and the function $f(x)$ which is given in Sec. II C, we obtain

$$\langle \xi_j | \tilde{p} | \xi_i \rangle = -i \int \langle \xi_j | x \rangle f^{-1}(x) \langle \xi_i | \rangle' dx + \frac{i}{2} \int \langle \xi_j | x \rangle f^{-2} \frac{df}{dx} \langle \xi_i | \rangle dx, \quad (27)$$

where the prime indicates differentiation. The matrix element $\langle \xi_j | \tilde{p} | \xi_i \rangle$ can be obtained by numerical integration of the above expression.

We can obtain the Floquet eigenstates, eigenvalues $e^{-i\Omega_\alpha T}$, and eigenphases Ω_α by constructing the Floquet evolution matrix and diagonalizing it. The Floquet evolution matrix is constructed by integrating the Schrödinger equation in Eq. (25) N times from $t=0$ to $t=T=2\pi/\omega$ with the initial conditions $|\Psi_\alpha(0)\rangle = \delta_{\alpha,j} |\xi_j\rangle$ ($j=1, \dots, N$), where the index α runs from 1 to N . We obtain $|\Psi_\alpha(T)\rangle$ which is expanded in terms of unperturbed states as $|\Psi_\alpha(T)\rangle = \sum_j a_{\alpha,j}(T) |\xi_j\rangle$ by diagonalizing the Floquet evolution matrix.

The Floquet eigenvalues of the scaled driven Morse system are obtained by performing the numerical calculations as describe above. Let us examine the scaled Floquet eigenvalue plots. Because the scaled Hamiltonian \tilde{H}_0 is not Hermitian, the time evolution matrix is not unitary. Therefore the Floquet eigenvalues do not have unit modulus except for the bound states. The lifetime of the complex quasi-bound states can be evaluated by writing the quasienergy $\Omega_\alpha = q_\alpha - i\Gamma_\alpha/2$, where $\tau_\alpha = 1/\Gamma_\alpha$ is the lifetime of state $|q_\alpha\rangle$. Figure 6 shows the scaled Floquet eigenvalues of the driven Morse potential for an external field strength $\varepsilon = 0.038$ a.u., and the frequency $\omega = 0.0925$ a.u. They are calculated for different rotated angles $\theta = 0.2$ and $\theta = 0.3$ with $x_s = 25$ a.u. We can see that the rotated continuum energies form the spirals from the origin out to the edge of the unit circle. The continuum energies are indicated by open circles. The spirals of continuum energies are not well defined near the origin due to numerical error. The filled circles indicate the quasibound states and their locations are invariant as the values of θ change. The quasi-bound state eigenvalues are independent of the scaling angles θ while the continuum eigenvalues rotate around the

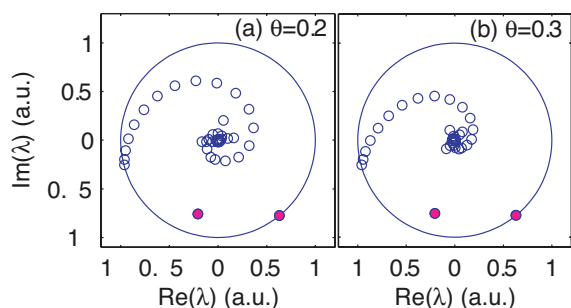


FIG. 6. (Color online) The Floquet eigenvalues for $\omega = 0.0925$ a.u., $\varepsilon = 0.038$ a.u. The eigenvalues are calculated by using ECCS with two different rotation angles $\theta = 0.2$ and $\theta = 0.3$ with $x_s = 35$ a.u. The rotated continuum energies are indicated by open circles. The filled circles indicate the quasibound states which do not sit on the spiral of the continuum and their locations are invariant as the values of θ change.

origin as θ is changed. It is important to note that in the numerical calculations, finite basis in the continuum are used by setting a hard wall at a location far from the origin of the potential. The calculation in Fig. 6 used 153 Morse basis states with the wall at $x = 141.60$ a.u., and gives the quasi-eigenvalues $\lambda_{\theta=0.2} = -0.205 - 0.759i$ and $0.630 - 0.776i$, and $\lambda_{\theta=0.3} = -0.206 - 0.755i$ and $0.629 - 0.773i$. The quasibound state energies depend weakly on the scaling angles and the position of the wall due to the fact that we use a discrete basis to represent the continuum.

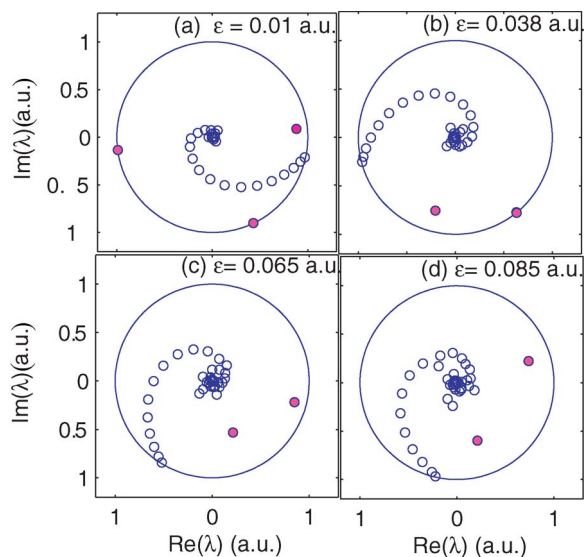


FIG. 7. (Color online) The Floquet eigenvalues for $\omega = 0.0925$ a.u. with four different field strengths (a) $\varepsilon = 0.01$ a.u., (b) $\varepsilon = 0.038$ a.u., (c) $\varepsilon = 0.065$ a.u., and (d) $\varepsilon = 0.085$ a.u. The eigenvalues are calculated by using ECCS with $\theta = 0.3$ and $x_s = 35$ a.u. The quasibound state eigenvalues are indicated by the filled circles. The rotated continuum energies are indicated by the open circles. At the field strength $\varepsilon = 0.01$ a.u., there exist three quasibound states. As the field strength increases, the number of the quasibound states decreases from 3 to 2.

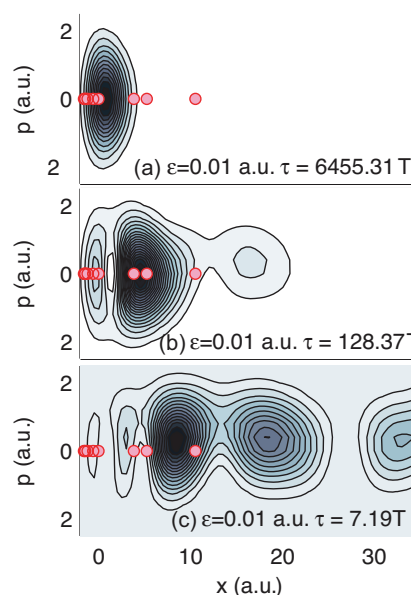


FIG. 8. (Color online) Husimi distribution of the three quasibound states for $\omega = 0.0925$ a.u. and $\varepsilon = 0.01$ a.u. For this weak field, the quasibound states almost resemble the bound states of the unperturbed Hamiltonian. The longest lifetime distribution still indicate the ground state. The second, and the third quasibound states remain the distributions of the first and second excited which couple with the continuum. Lifetimes for each stat are given in the unite of the driving field period $T = 2\pi/\omega$. The locations of the period-1 periodic orbits are indicated by filled circles.

Let us now consider the behavior of the quasibound states as the field increases. Figure 7 shows the Floquet eigenvalues for the field frequency $\omega = 0.0925$ a.u. with four different field strengths $\varepsilon = 0.01$ a.u., $\varepsilon = 0.038$ a.u., $\varepsilon = 0.065$ a.u., and $\varepsilon = 0.085$ a.u. These were obtained by using ECCS with $\theta = 0.3$ and $x_s = 35$ a.u. The quasibound state eigenvalues are indicated by the filled circles. At the lowest field strength $\varepsilon = 0.01$ a.u., there are three quasibound states which correspond to destabilized bound states of the unperturbed Hamiltonian. As we increase the external field intensity, the number of quasibound states decreases to 2. This result is consistent with Ben-Tal *et al.* [11] who studied the Morse system interacting with a field. They explained this by using the dressed potential approach and showed that the dressed Morse potential could support less bound states as the field strength is increased.

Husimi distributions of the quasibound states at the frequencies and field strengths corresponding to the Figs. 7(a)–7(c) are shown in Figs. 8–10. Lifetimes for each state are given in the units of the driving field period $T = 2\pi/\omega$. The locations of period-1 periodic orbits in the underlying classical phase space are indicated by filled circles. The period-1 periodic orbits are the orbits that return to their starting points in phase space after one period of the field. They were obtained by integrating the equations of motion $\dot{x} = \partial H / \partial p$ and $\dot{p} = -\partial H / \partial x$ up to $t = T$, and use the root finding method along the x axis ($p = 0$) to find the fixed points which satisfy the conditions $x(T) = x(0)$ and $p(T) = p(0) = 0$. We note that these period-1 periodic fixed points are also the solutions

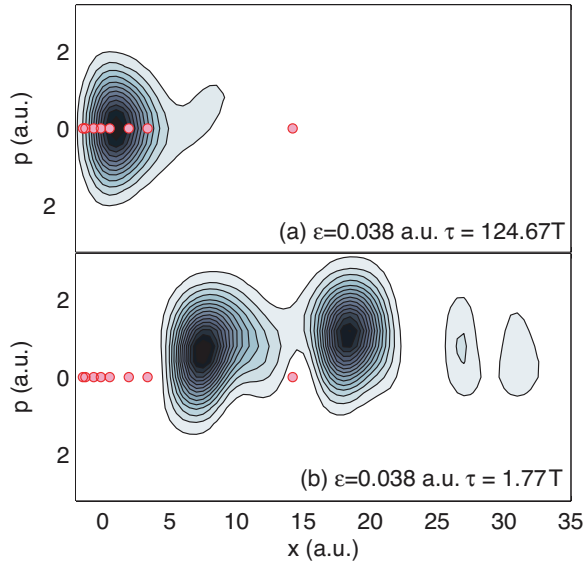


FIG. 9. (Color online) Husimi distribution of the three quasibound states for $\omega=0.0925$ a.u. and $\varepsilon=0.038$ a.u. Lifetimes for each stat are given in the units of the driving field period $T=2\pi/\omega$. The locations of the period-1 periodic orbits are indicated by filled circles.

to $x(nT)=x(0)$, and $p(nT)=p(0)$ for any integer n . This means that the orbits will also come back to their starting points after each n periods of the driving field. At the low value of field strength $\varepsilon=0.01$ a.u. (Fig. 8), the Husimi distributions of the quasibound states look similar with the three bound state Husimi distributions except that the second and third quasibound states have developed elongated distributions due to their coupling to the continuum. The quasibound state originating from the ground state has a very long life-

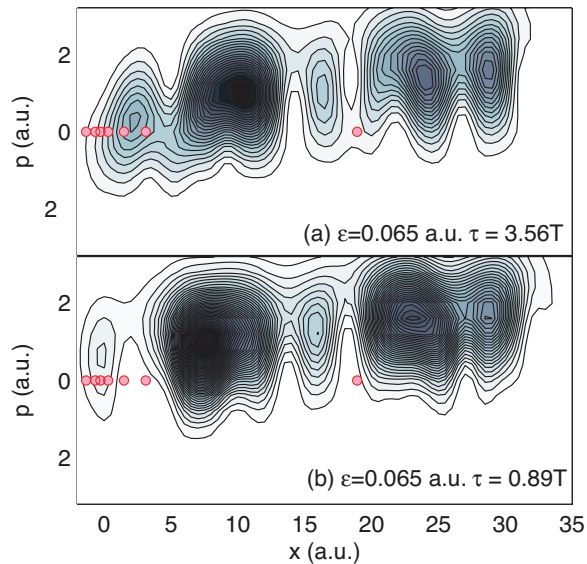


FIG. 10. (Color online) Husimi distribution of the three quasibound states for $\omega=0.0925$ a.u. and $\varepsilon=0.065$ a.u. Lifetimes for each stat are given in the unite of the driving field $T=2\pi/\omega$. The locations of the periodic orbits are indicated by filled circles.

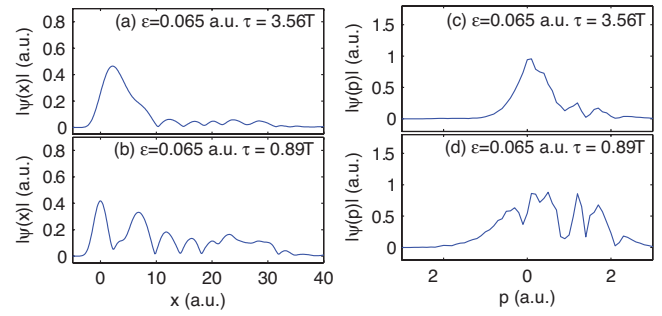


FIG. 11. (Color online) Plots (a) and (b) give the probability distributions in configuration space, and plots (c) and (d) give the probability distributions in momentum space of the two quasibound states for the system with $\varepsilon=0.065$ a.u.

time $\tau=6455.31T$. For the field strength $\varepsilon=0.038$ a.u. (Fig. 9), the longest living state still resembles the ground state. However, for the shorter living state, the probability begins to shift to larger values of x and to positive values of momentum. It also occupies the neighborhood of the outermost period-1 unstable periodic orbit in the underlying classical phase space. This unstable periodic orbit was pushed out toward the larger values of x with the stronger field. As we increase the field strength to $\varepsilon=0.065$ a.u. (Fig. 10), both quasibound states are shifted to positive momentum. This appears to be a clear indication that the heteroclinic tangle shown in Fig. 4 is strongly influencing the behavior of the quasibound states. The lifetimes of the quasibound state decrease with increasing values of the external field strength.

In order to show this shift of probability to positive momentum more clearly, in Fig. 11 we separately plot the probability distributions in configuration space and momentum space of the two quasibound states for $\varepsilon=0.065$ a.u. Thus, it appears that the heteroclinic tangles for the driven Morse system do influence and give support to quasibound state structures in open space. This is consistent with similar results for waveguide structures in Ref. [23].

V. CONCLUSIONS

We have studied the dynamics of the driven Morse system in a strong time-periodic field. We use Floquet theory and the exterior complex scaling method to find the quasibound states of the system. The quasibound state eigenvalues are independent of the scaling angle and their behavior under complex coordinate rotation is different from the behavior of the continuum Floquet eigenenergies. The invariance of the quasibound states is shown as the scaling angle is varied. We found that as the external field strength is increased from $\varepsilon=0.01$ to 0.085 a.u., the number of the quasibound states decreases from three to two and the quasibound states become less stable. This result is different from the inverted Gaussian potential system, which shows the increased number of quasibound states and increased stability of at least one quasibound state as the strength of the external field increases [11].

The classical phase-space plots show that the outer unstable periodic fixed point was pushed outward while the next inner unstable periodic fixed point was pushed slightly inward to smaller values of x as the field increases. We found that most of the probability in Husimi distributions of quasi-bound states lies between the two outermost period-1 unstable periodic orbits and is shifted to positive momentum, which is consistent with having support on the heteroclinic tangles of this system.

ACKNOWLEDGMENTS

The authors thank the Robert A. Welch Foundation (Grant No. F-1051) and the Engineering Research Program of the Office of Basic Energy Sciences at the U.S. Department of Energy (Grant No. DE-FG03-94ER14465) for support of this work. L.E.R. also thanks the Office of Naval Research (Grant No. N00014-03-1-0639) for partial support of this work. The authors also thank the Texas Advanced Computing Center (TACC) for use of their computer facilities.

-
- [1] M. Pont and M. Gavrilă, Phys. Rev. Lett. **65**, 2362 (1990).
 - [2] M. P. deBoer, J. H. Hoogenraad, R. B. Vrijen, L. D. Noordam, and H. G. Muller, Phys. Rev. Lett. **71**, 3263 (1993).
 - [3] M. P. deBoer, J. H. Hoogenraad, R. B. Vrijen, R. C. Constantinescu, L. D. Noordam, and H. G. Muller, Phys. Rev. A **50**, 4085 (1994).
 - [4] Q. Su, J. H. Eberly, and J. Javanainen, Phys. Rev. Lett. **64**, 862 (1990).
 - [5] Q. Su and J. H. Eberly, J. Opt. Soc. Am. B **7**, 564 (1990).
 - [6] R. Grobe and C. K. Law, Phys. Rev. A **44**, R4114 (1991).
 - [7] J. H. Eberly and K. C. Kulander, Science **64**, 1229 (1993).
 - [8] J. N. Bardsley and M. J. Comella, Phys. Rev. A **39**, 2252 (1989).
 - [9] N. Ben-Tal, N. Moiseyev, R. Kosloff and C. Cerjan, J. Phys. B **26**, 1445 (1993).
 - [10] N. Ben-Tal, N. Moiseyev, and R. Kosloff, Phys. Rev. A **48**, 2437 (1993).
 - [11] N. Ben-Tal, N. Moiseyev, and R. Kosloff, J. Chem. Phys. **98**, 9610 (1993).
 - [12] T. Timberlake and L. E. Reichl, Phys. Rev. A **64**, 033404 (2001).
 - [13] Agapi Emmanouilidou and L. E. Reichl, Phys. Rev. A **65**, 033405 (2002).
 - [14] Agapi Emmanouilidou, C. Jung, and L. E. Reichl, Phys. Rev. E **68**, 046207 (2003).
 - [15] R. B. Walker and R. K. Preston, J. Chem. Phys. **67**, 2017 (1977).
 - [16] M. E. Goggin and P. W. Milonni, Phys. Rev. A **37**, 796 (1988).
 - [17] J. J. Tanner and M. M. Maricq, Phys. Rev. A **40**, 4054 (1989).
 - [18] J. Heagy and J. M. Yuan, Phys. Rev. A **41**, 571 (1990).
 - [19] R. Graham and M. Höhnerbach, Phys. Rev. A **43**, 3966 (1991).
 - [20] C. Jung, *The Electron*, edited by D. Hestenes and A. Weingartshofer (Kluwer Academic Publishers, Netherlands, 1991), pp. 219–238.
 - [21] W. P. Reinhardt, Annu. Rev. Phys. Chem. **33**, 223 (1982).
 - [22] N. Moiseyev, Phys. Rep. **302**, 211 (1998); J. Phys. B **31**, 1431 (1998).
 - [23] Hoshik Lee, C. Jung, and L. E. Reichl, Phys. Rev. B **73**, 195315 (2006).
 - [24] L. E. Reichl, *The Transition to Chaos: Conservative Classical Systems and Quantum Manifestations*, 2nd ed. (Springer-Verlag, Berlin, 2004).
 - [25] K. Takahashi, Prog. Theor. Phys. Suppl. **98**, 109 (1989); Y. Chun and H. Lee, Annu. Rev. Phys. Chem. **307**, 483 (2003).
 - [26] J. N. Bardsley, A. Szoke, and M. J. Cormella, J. Phys. B **21**, 3899 (1988).
 - [27] M. Matsumoto, J. Phys. B **21**, 2863 (1988).